RSC Advances

PAPER

View Article Online
View Journal | View Issue

Cite this: *RSC Adv.*, 2020, **10**, 41993

Effects of the surface polarity of nanomaterials on their interaction with complement protein gC1q†

Shuai Wang,[ab] Xinwen Ou,[b] Yanee Wutthinitikornkit,[b] Ming Yi*[ac] and Jingyuan Li *[b]

There are increasing studies about the biocompatibility of nanomaterials (NMs) as their applications in biomedicine become more widespread. The biocompatibility of NMs involves the recognition by the immune system including complement protein gC1q. In this work, the interaction of graphene oxide (GO) and self-assembled monolayer (SAM)-coated gold (111) surface with gC1q was studied by molecular dynamics (MD) simulations. The impacts of surface polarity of GO on its interaction with gC1q and the possible immune response were discussed by comparing the binding behavior of gC1q to the GO sheets with different oxidation degrees (*i.e.*, $C_5O_1(OH)_1$ and $C_{20}O_1(OH)_1$). We find the ghB module of gC1q tends to bind to GO sheet ($C_5O_1(OH)_1$) with strong surface polarity, as the ghB module forms more hydrogen bonds with this GO sheet. On the other hand, the ghC module of gC1q tends to bind to GO ($C_{20}O_1(OH)_1$) with weak surface polarity, as the ghC module tends to form pi–pi stacking and stronger hydrophobic interaction with this GO sheet. Similar phenomena are also found in the adsorption of gC1q with SAM: ghC prefers to bind to hydrophobic CH_3-SAM, and ghB prefers to bind to charged COO-SAM. The different binding modules of gC1q may result in different activation levels of complement system. Our findings suggest that the surface polarity of NMs regulates the interaction of NMs with gC1q and the subsequent immune response. In other words, the biocompatibility of NMs may be regulated by adjusting their surface polarity.

Received 23rd June 2020
Accepted 8th November 2020

DOI: 10.1039/d0ra05493c

rsc.li/rsc-advances

Introduction

Because of their applications in biomedicine and biotechnology,[1–8] the studies on the biocompatibility of nanomaterials (NMs), especially graphene oxide (GO)[9–12] and self-assembled monolayer (SAM) modified surfaces,[13–15] have received intensive attention. One important factor affecting the biocompatibility of NMs is their interaction with the immune system and the resulting immunological effects.[16–21] There is growing evidence that the immunological effects of NMs are influenced by their surface polarity.[17,22,23] For example, the polyvinyl alcohol-coated poly(lactic-*co*-glycolic acid) (PLGA) nanoparticles (PLGA-NPs) with neutral surface show higher phagocytosis than charged PLGA-NPs coated with chitosan or poloxamer 188.[17] And there have been a variety of experimental works showing the impacts of oxidation degree of GO on the interaction with proteins and the resulting inflammation response and cytotoxicity in macrophages.[24–28]

The complement system consisting of three complement pathways (*i.e.*, classical, alternative and lectin pathway) is an important part of human immune system. The activation of immune response through the classical complement pathway is initiated by complement protein gC1q when it senses foreign intruders.[29] gC1q is composed of three modules, *i.e.*, ghA, ghB, and ghC. Both ghB and ghC modules can recognize foreign intruders, though the immune response initiated by ghB is stronger than that by ghC.[30] There are two distinct recognition modes of gC1q with foreign intruders: ghC module is likely to have a central role in the binding of gC1q with hydrophobic targets,[31,32] and gC1q bind polyanions is largely dependent on the ghB module.[31,33] Therefore, the surface properties of foreign intruders, especially the surface polarity, should affect the recognition mode of gC1q and subsequent activation level of complement system. Thielens *et al.*[34] found that only anionic polydiacetylene micelles can bind complement proteins and activate the complement system. Wibroe *et al.*[35] found that the activation level of complement system is positively correlated with the oxidation degree of GO.

Molecular dynamics (MD) simulations have been widely used to study the interaction between NMs and immune-related proteins and to discuss the impacts of surface properties of NMs. For example, Yu *et al.*[36] investigated the interaction of both pristine and modified fullerenes with leukocyte common antigen (CD45) and found their distinct binding modes. Xie

[a]College of Informatics, Huazhong Agricultural University, Wuhan 430070, China
[b]Department of Physics, Zhejiang University, Hangzhou 310027, China. E-mail: jingyuanli@zju.edu.cn
[c]School of Mathematics and Physics, China University of Geosciences, Wuhan 430074, China. E-mail: mingyi@cug.edu.cn

† Electronic supplementary information (ESI) available. See DOI: 10.1039/d0ra05493c

et al.[37] studied the adsorption behavior of lysozyme which plays an important immunomodulatory role in human innate immune system,[38] and they explored the effects of surface polarities of self-assembled monolayer (SAM) on Au (111) on their interaction with lysozyme. In addition, previous computational studies on the interaction of NMs with the complement protein gC1q investigated the effects of the size of NMs on the binding stability of gC1q.[39] To our knowledge, there are no computational researches on the interaction mode between gC1q and NMs, especially the comparison of two recognition modules, *i.e.*, ghB and ghC modules. The impacts of the surface polarities of NMs on the recognition behavior of gC1q and the resulting immune response remain largely elusive.

In this study, MD simulations were performed to investigate the interaction of complement protein gC1q with the GO sheet and self-assembled monolayer (SAM)-coated gold (111) surface. We focused on the impacts of the surface polarity of the GO and SAM on the binding mode of gC1q as well as the corresponding immune response. The ghB module of gC1q recognizes GO with high oxidation degree ($C_5O_1(OH)_1$), whereas the ghC module of gC1q recognizes GO with low oxidation degree ($C_{20}O_1(OH)_1$). There are up to 22 charged residues distributed on the surface of ghB module engendering the preference for GO with higher polarity. Such recognition mode may trigger strong complement activation level and immune response. On the other hand, the surface of ghC module shows a predominance of non-polar residues (~40%) including several aromatic residues. Thus, ghC can form pi–pi stacking and hydrophobic interaction with the GO with lower polarity and induce a weak immune response. Similar phenomena are also found for gC1q adsorption on self-assembled monolayer (SAM)-protected gold nanoparticle with distinct surface polarities (*i.e.* hydrophobic CH_3-SAM and charged COO-SAM). The ghB prefers to bind to COO-SAM, and the ghC prefers to bind to the CH_3-SAM. Our results suggest that the recognition mode of gC1q and the activation of corresponding immune response can be modulated by turning the surface polarity of GO and SAM.

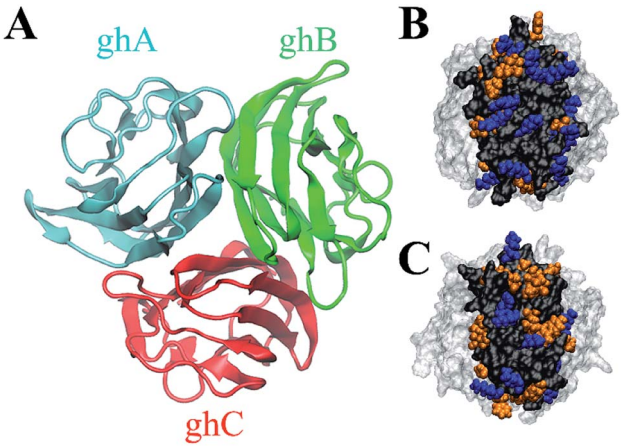

Fig. 1 Top view of the structure of gC1q, comprising three modules: ghA (cyan), ghB (green) and ghC (red) (A). Side view of the hydrophobic (orange) and positively charged (blue) residues on the surface of two binding modules (highlighted in black) of gC1q: ghB (B) and ghC (C).

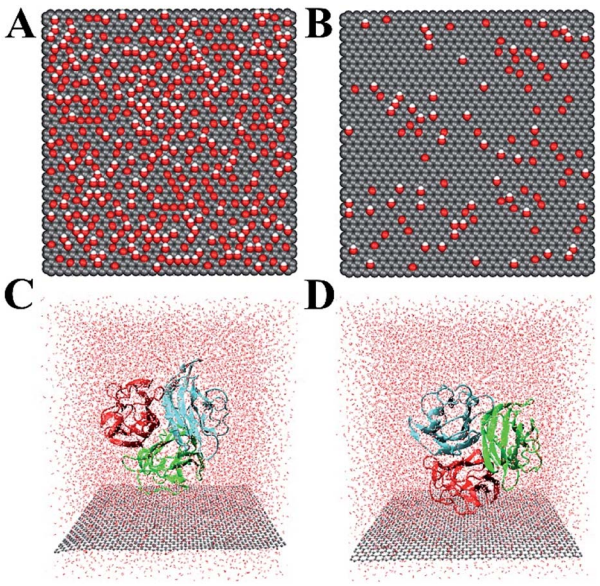

Fig. 2 Top view of the graphene oxide: $C_5O_1(OH)_1$ (A) and $C_{20}O_1(OH)_1$ (B). Atoms in graphene oxide sheet are shown as vdW spheres (C: gray, O: red, H: white). The initial configurations of protein gC1q with ghB (C) and ghC (D) facing the GO sheet. Water molecules are shown as red dots.

Methods

A. Protein and surface models

The crystal structure of gC1q protein was obtained from the Protein Data Bank (PDB ID: 1PK6 (ref. 40)). As shown in Fig. 1A, gC1q protein is a compact, almost spherical heterotrimeric assembly consisting of 394 residues. As the O/C ratio of graphene oxide (GO) can be effectively adjusted in a range of ~11–~51% in experiments,[41–44] two kinds of GO sheets with distinct O/C ratios, *i.e.*, $C_5O_1(OH)_1$ (Fig. 2A), and $C_{20}O_1(OH)_1$ (Fig. 2B) were constructed based on the Lerf–Klinowski model.[45] The oxygen-containing groups (epoxy and hydroxyl functional groups) were randomly distributed on both sides of the GO sheet. Both kinds of GO sheets have the same size of 7.1 × 7.5 nm^2. In addition, self-assembled monolayer (SAM)-protected gold nanoparticles with distinct surface polarities were constructed using 10-amino-1-decanethiol (–$S(CH_2)_{10}$-R), where R stands for a functional group, *i.e.* –CH_3, –COO. All alkanethiol chains of SAM were packed on the gold (111) surface with a $\sqrt{3} \times \sqrt{3}$ lattice structure.[46,47] And all the SAMs have dimensions of 7.2 nm × 7.4 nm.

B. MD simulations

In our simulations, OPLS-AA force field[48] was applied for the protein and SAM. We adopted the force field for graphene nanosheets and oxygen-containing groups from previous studies,[49,50] wherein the sp^2 carbon atoms were modelled as uncharged Lennard-Jones particles with σ = 0.340 nm and a depth of potential well ε = 0.233 kJ mol^{-1}. The GO is electrically neutral. Detailed force field parameters of sp^3-hybridized

carbon, hydroxyl and epoxy groups are described in the Table S1.†

The ghB and ghC modules of gC1q were facing the two GO surfaces (Fig. 2C and D) separately to obtain four different initial configurations of gC1q on the GO sheet (*i.e.*, ghB/$C_5O_1(OH)_1$, ghB/$C_{20}O_1(OH)_1$, ghC/$C_5O_1(OH)_1$, and ghC/$C_{20}O_1(OH)_1$). The initial closest distance of heavy atoms between the protein and GO is 0.5 nm. All gC1q/GO systems were embedded in a box of 7.4 × 7.7 × 8.5 nm^3 and solvated with TIP3P[51] water molecules. The distance between the protein or GO sheet and the boundary of the box was at least 1.0 nm. Afterwards, nine chloride ions were added to neutralize the system, and then appropriate numbers of chloride and sodium ions were added to reach a physiological salt concentration of 0.15 M at neutral pH. Finally, all the simulations were performed using GROMACS 2018.3 package.[52]

For each run, the simulation was first energy-minimized by using the steepest descent method, and then the system was pre-equilibrated with a 1 ns equilibration in the NVT ensemble to relax the solvent molecules with position restraints imposed on the GO sheet and the backbone of protein. After that, the system was pre-equilibrated with 1 ns constant pressure equilibration in the NPT ensemble. Finally, production run was performed in the NPT ensemble for 50 ns. The temperature of all systems was maintained at 310 K using a v-rescale thermostat[53] with a 0.1 ps coupling constant, and the pressure was kept at 1 bar with semi-isotropic coupling directions ($X + Y$, Z) using the Berendsen's algorithm.[54] The standard periodic boundary conditions (PBC) were applied in all directions (X, Y and Z). Solute bonds involving hydrogen atoms were constrained by the LINCS algorithm.[55] Both the van der Waals (vdW) interaction and real-space Coulomb interaction were calculated using a cutoff distance of 1.0 nm, while the long-range electrostatic interaction was handled by the particle mesh Ewald (PME) method.[56] For all simulations, the integration time step was 2.0 fs, and snapshot was recorded every 5 ps. The neighbor list generated with a cutoff distance of 1.0 nm was updated every 20 steps. Visualization and analysis of MD trajectories were implemented by VMD1.9.3.[57]

Results and discussion

We first investigated the adsorption of gC1q with its ghB module facing the graphene oxide (GO) sheets. The adsorption on $C_5O_1(OH)_1$ and $C_{20}O_1(OH)_1$ was studied separately. And the number of contacts with GO was calculated to illustrate the adsorption process (a contact is counted when a heavy atom in the protein is within 0.5 nm of a carbon/oxygen atom in GO). It should be noted that the contacts of gC1q are totally attributed to ghB.

As shown in Fig. 3A, the number of contacts of gC1q increases in a stepwise manner as the adsorption proceeds. For example, during the adsorption process on $C_5O_1(OH)_1$, the number of contacts progressively increases to ~100 (t = 2.5 ns), ~200 (t = 6 ns), and ~229 (t = 23 ns). Similar adsorption process is also exhibited on $C_{20}O_1(OH)_1$. In both systems, the number of contacts reaches a plateau after t = 25 ns. And the

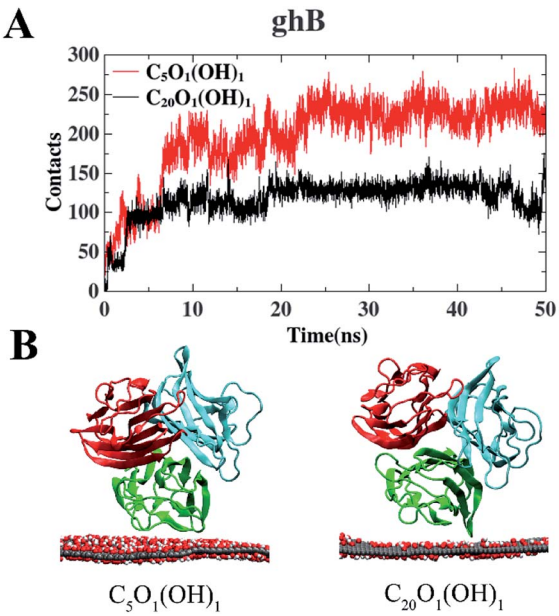

Fig. 3 The number of contact heavy atoms of gC1q (ghB) with GO (A). Representative structures of gC1q with ghB adsorbed on GO (B).

average numbers of contacts over the interval of t = 25 ns to 50 ns are 229.9 ($C_5O_1(OH)_1$) and 123.0 ($C_{20}O_1(OH)_1$). This suggests that the adsorption of ghB on $C_5O_1(OH)_1$ is stronger than on $C_{20}O_1(OH)_1$. The distinct adsorption behaviors are also reflected in the representative snapshots of the adsorbed protein. ghB module adopts flat structure and establishes more intimate contact with $C_5O_1(OH)_1$ than with $C_{20}O_1(OH)_1$ (Fig. 3B).

The interaction energies between ghB and GO sheets were also calculated. The Coulomb interaction potential of ghB module with $C_5O_1(OH)_1$ (−192.9 kJ mol^{-1}) is stronger than that with $C_{20}O_1(OH)_1$ (−25.4 kJ mol^{-1}). In addition, the average number of hydrogen bonds formed between ghB module and $C_5O_1(OH)_1$ is 7.5, much higher than that formed with $C_{20}O_1(OH)_1$ (0.7). Taken together, the binding preference of the ghB module for $C_5O_1(OH)_1$ is largely attributed to the favorable electrostatic interaction.

We also studied the adsorption behavior of gC1q with its ghC module initially facing the GO sheets. In these cases, the contacts of gC1q with GO are totally attributed to the ghC module. As shown in Fig. 4A, the numbers of contacts of ghC with both GO sheets reach a plateau before t = 30 ns. Thereafter they oscillate around the mean values of ~213 ($C_{20}O_1(OH)_1$) and ~141 ($C_5O_1(OH)_1$). Besides, the interaction energy between ghC and $C_{20}O_1(OH)_1$ is stronger than that between ghC and $C_5O_1(OH)_1$ (−411.1 kJ mol^{-1} *vs.* −320.5 kJ mol^{-1}). Such difference is mainly attributed to the stronger van der Waals energy between ghC and $C_{20}O_1(OH)_1$ than that between ghC and $C_5O_1(OH)_1$ (−311.8 kJ mol^{-1} *vs.* −217.6 kJ mol^{-1}). In order to comprehensively evaluate the binding stability of protein, we further calculated free energy of protein binding using MM-PBSA method.[58] The binding free energy between ghC and $C_{20}O_1(OH)_1$ is also stronger than that between ghC and $C_5O_1(OH)_1$ (−368.9 kJ mol^{-1} *vs.* −308.2 kJ mol^{-1}).

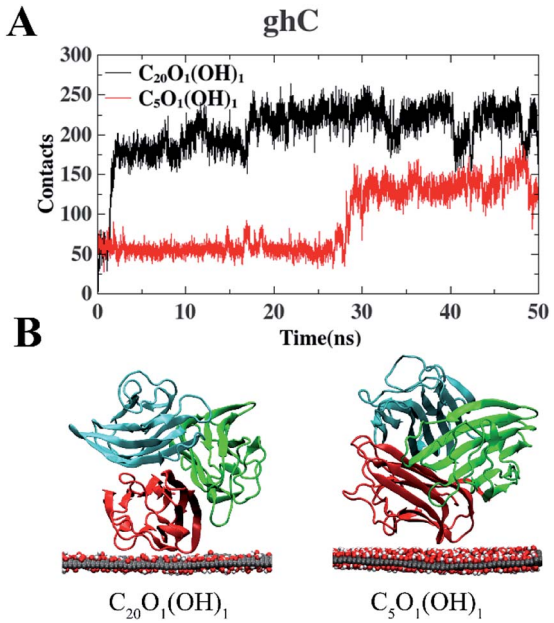

Fig. 4 The number of contact heavy atoms of gC1q (ghC) with GO (A). Representative structures of gC1q with ghC adsorbed on GO (B).

Consequently, gC1q can adsorb on GO sheets through its ghC module. And the adsorption on $C_{20}O_1(OH)_1$ is clearly stronger than on $C_5O_1(OH)_1$. As can be seen in the representative snapshots of the adsorbed protein, ghC module adopts flat configuration and establishes more intimate contact with $C_{20}O_1(OH)_1$ than with $C_5O_1(OH)_1$ (Fig. 4B).

While there are more contact atoms of ghC with $C_{20}O_1(OH)_1$ than with $C_5O_1(OH)_1$, the Coulomb interaction potential of ghC with these two GO sheets are very close: -102.9 kJ mol^{-1} ($C_5O_1(OH)_1$) *vs.* -99.3 kJ mol^{-1} ($C_{20}O_1(OH)_1$). In addition, the average numbers of hydrogen bonds formed between ghC and oxygen-containing groups on GO sheets are also modest: 4.5 ($C_5O_1(OH)_1$) *vs.* 3.7 ($C_{20}O_1(OH)_1$). In short, the interaction between polar groups, *e.g.* hydrogen bond interaction, may not account for the distinct adsorption behaviors of ghC on these two GO sheets. The binding preference of ghC for $C_{20}O_1(OH)_1$ with weak surface polarity may be attributed to the hydrophobic interaction.

Taken together, gC1q exhibits distinct behaviors on GO sheet with various oxidation degrees: the ghB module of gC1q prefers to bind to GO sheet with high oxidation degree ($C_5O_1(OH)_1$), whereas the ghC module of gC1q tends to bind to GO sheet with low oxidation degree ($C_{20}O_1(OH)_1$). In other words, the binding modes of gC1q are markedly affected by surface polarity of GO sheet.

In order to further validate the impacts of the surface polarity of nanomaterials on their interaction with gC1q, we have also studied the binding behavior of gC1q on self-assembled monolayer (SAM)-protected gold nanoparticles with two distinct surface polarities (*i.e.* hydrophobic CH_3-SAM and charged COO-SAM). The number of contacts of gC1q was calculated to compare the binding preference of the protein. It can be seen from Fig. S2† that the average number of contacts of ghC with the CH_3-SAM is significantly higher than that with the COO-SAM (17.0 *vs.* 0). This result suggests that ghC prefers to bind to the hydrophobic SAM, which is consistent with the result that ghC prefers to bind to $C_{20}O_1(OH)_1$ with weak surface polarity. As for the case of ghB (Fig. S1†), the average number of contacts with SAMs are 34.9 (COO-SAM) and 9.8 (CH_3-SAM), separately. The binding preference of ghB to COO-SAM is considerably higher than that to CH_3-SAM, which is also in agreement with the result that ghB prefers to bind to $C_5O_1(OH)_1$ with more oxidized groups. The results of both SAM and GO suggest that the surface polarity of nanomaterials affect the adsorption mode of gC1q: the ghC prefers to bind to nanomaterials with weak surface polarity, and the ghB prefers to bind nanomaterials with strong surface polarity.

We notice the adsorption behavior of protein in response to the surface polarity of GO and SAM is largely ascribed to the distinct residue composition (*i.e.*, positively charged, negatively charged, polar, and non-polar residues) of the surface of ghB and ghC modules (Table S2†). Charged residues are more abundant on the surface of ghB than on the surface of ghC (22 *vs.* 16), especially positively charged residues (14 *vs.* 9). On the other hand, the number of non-polar residues in ghC is much higher than in ghB (27 *vs.* 18). The distinct residue composition is also illustrated in Fig. 1B and C. In short, ghC exhibits much lower surface polarity than ghB.

To further study the relationship between the surface residue composition of gC1q and its adsorption behavior on the GO sheet with varying surface polarity, the number of contact residues (*i.e.*, the contact residues are the ones that establish at least one contact atom with GO sheet) with GO sheets were assessed. We focused on the two preferential binding modes, *i.e.*, ghB module on $C_5O_1(OH)_1$ and ghC module on $C_{20}O_1(OH)_1$. In the case of ghB on $C_5O_1(OH)_1$, the average number of positively charged, negatively charged, polar, and non-polar residues in contact with GO are 6.5, 3.0, 3.0, and 1.9, respectively (Fig. 5A). Clearly, there are much more positively charged residues contacting with this GO than the other three types of residues. The fraction of positively charged residues in the contact residues is 45.1% (6.5 out of 14.4), considerably higher than their "intrinsic" proportion (22.9%, 14 out of 61) on the surface of ghB. Hence, the positively charged residues are preferred in this binding mode.

We further identified the highly-involved residues (*i.e.*, the residues with the contact probability more than 50%). As can be seen in Fig. 5C, the highly-involved residues include six positively charged residues (Arg108, Arg109, Arg114, Arg129, Lys132 and Arg163), three negatively charged residues (Asp110, Glu127 and Glu162) as well as three polar residues (Gln111, Ser130 and Gln198) and two non-polar residues (Val105 and Pro106). As mentioned above, the binding mode of ghB to $C_5O_1(OH)_1$ is mainly attributed to a favorable electrostatic interaction. The results about the highly-involved residues also agree with previous experimental study, wherein the ghB module mainly recognizes foreign intruders through the charged residues (*i.e.*, Arg114, Arg129, Arg163, and Glu162).[31,33] Our simulation further suggests that three positively charged residues (*i.e.* Arg108,

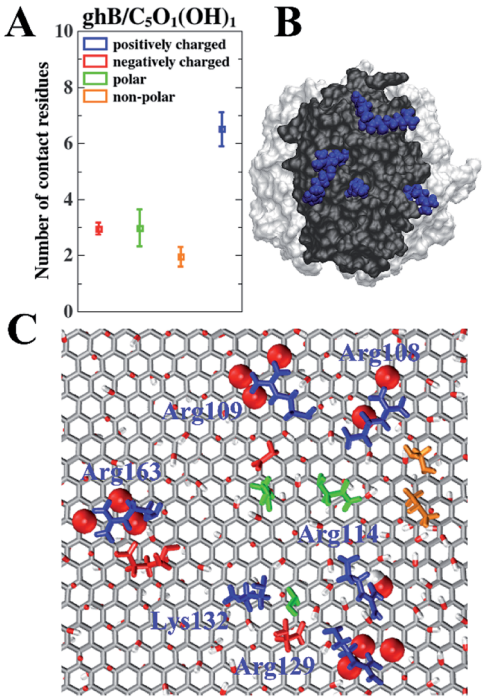

Fig. 5 The number of contact residues of ghB module with the $C_5O_1(OH)_1$ (A). Location of the positively charged residues of ghB module (highlighted as blue region in black surface) adsorbed on $C_5O_1(OH)_1$ (B). Top view of the highly-involved residues whose contact probability is more than 50% (C). The sidechains of adsorbed residues are shown in licorice representation following the same color scheme in (A).

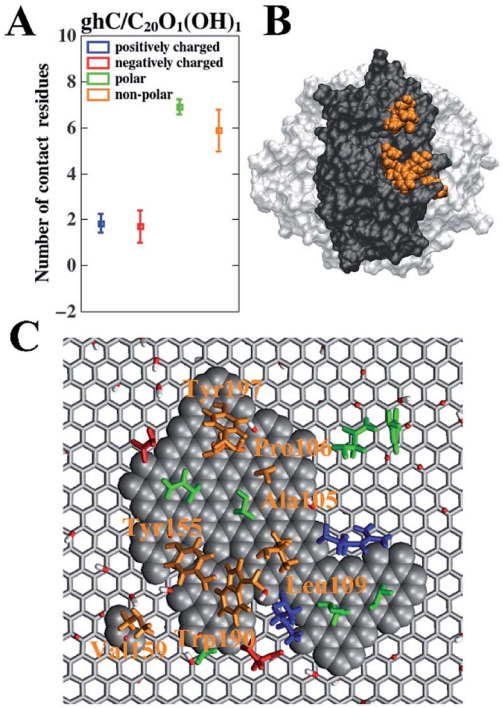

Fig. 6 The number of contact residues of ghC module with $C_{20}O_1(OH)_1$ (A). Location of the contact non-polar residues of the ghC module (highlighted as yellow region in black surface) with $C_{20}O_1(OH)_1$ (B). Top view of the highly-involved residues whose contact probability is more than 50% (C). The adsorbed residues are shown in licorice representation following the same color scheme in (A).

Arg109 and Lys132) may also be involved in the intruder recognition. Therefore, the adsorption of ghB on $C_5O_1(OH)_1$ is mainly through its charged residues, especially the positively charged ones.

Such binding mode is also consistent with the nature of $C_5O_1(OH)_1$ with strong surface polarity: there are more hydroxyl groups and epoxy groups on $C_5O_1(OH)_1$ than on $C_{20}O_1(OH)_1$. And there are more charged residues distributed on the surface of ghB module than on ghC (22 *vs.* 16). These charged residues, especially positively charged ones (Fig. 5B) form favorable electrostatic interaction with the hydroxyl groups and epoxy groups of GO (Fig. 5C, highlighted as vdW spheres). Hence, the Coulomb interaction potential of ghB on $C_5O_1(OH)_1$ is stronger than on $C_{20}O_1(OH)_1$ (-192.9 kJ mol^{-1} *vs.* -25.4 kJ mol^{-1}).

Taken together, the binding preference of ghB module for $C_5O_1(OH)_1$ is mainly owing to a favorable interaction through hydrogen bonds. Similar phenomenon was also found for the adsorption of virus protein R (Vpr13-33) from HIV-1 on GO, whose adsorption affinity is also attributed to its positively charged residues.[59]

As for ghC on $C_{20}O_1(OH)_1$, the average numbers of the positively charged, negatively charged, polar, and non-polar contact residues are 1.9, 1.7, 6.9, and 5.9, respectively (Fig. 6A). Clearly, there are much more non-polar and polar residues contacting with GO than charged residues. In addition, we find the number of non-polar and polar contact residues of ghC on $C_{20}O_1(OH)_1$ are 3.1 times (5.9 *vs.* 1.9) and 2.3 times (6.9 *vs.* 3.0) more than that of ghB on $C_5O_1(OH)_1$. On the other hand, the number of charged contact residues of ghC on $C_{20}O_1(OH)_1$ is only 37.8% (3.6 *vs.* 9.5) of ghB on $C_5O_1(OH)_1$. Apparently, non-polar and polar residues are preferred for this binding mode.

We also analyzed the highly-involved residues responsible for their adsorption following the same criterion described above. As can be seen in Fig. 6C, the highly-involved residues include seven non-polar residues (Ala105, Pro106, Leu109, Tyr155, Val159, Trp190 and Tyr197), seven polar residues (His101, Gln102, Asn107, Ser108, Ser126, Thr127 and Ser157) as well as two positively charged residues (Arg111 and Lys129) and two negatively charged residues (Glu188 and Asp195). The results about the highly-involved residues agree well with previous experimental study, wherein ghC module recognizes hydrophobic targets through its non-polar residues (*i.e.*, Ala105, Pro106, Tyr155 and Trp190).[31,32] Our simulation further indicates that three non-polar residues (Tyr197, Leu109, and Val159) may also be involved in the intruder recognition. Hence, the adsorption of ghC on $C_{20}O_1(OH)_1$ is mainly through its non-polar residues. Such binding mode is consistent with the nature of $C_{20}O_1(OH)_1$, featuring weak surface polarity. And there are more non-polar residues distributed on the surface of ghC than on ghB (27 *vs.* 18). As a result, of the highly-involved residues of ghC, all seven non-polar (Fig. 6B, highlighted in orange) and 57.1% polar residues (4 out of 7) bind to the non-oxidized region

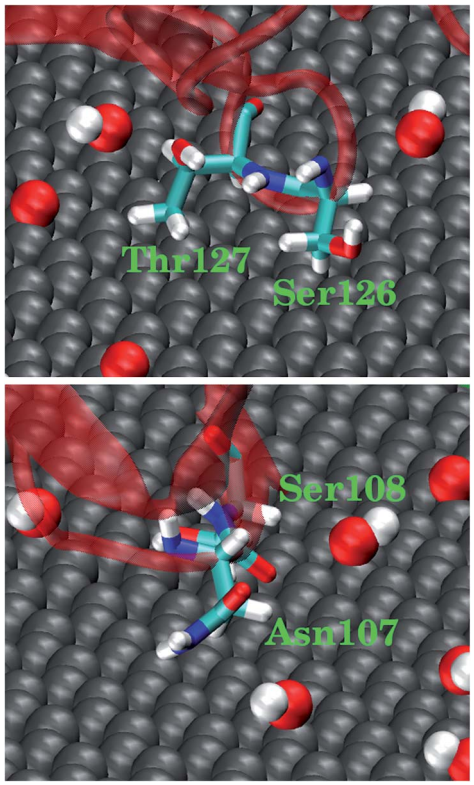

Fig. 7 Representative snapshots for four polar residues in ghC adsorbed on $C_{20}O_1(OH)_1$. The polar residues contact the non-oxidized region of GO through their hydrophobic carbonaceous groups.

of GO (Fig. 6C, highlighted as vdW grey spheres). And these polar residues mainly bind to the non-oxidized region of GO through their hydrophobic carbonaceous groups (Fig. 7).

In order to illustrate the interaction of highly-involved residues of ghC module with $C_{20}O_1(OH)_1$ in a more quantitative way, we calculated the interaction energies of different types of these residues (*i.e.*, positively charged, negatively charged, polar, and non-polar residues) with $C_{20}O_1(OH)_1$. The interaction energy of uncharged residues is stronger than charged residues (-186.4 kJ mol^{-1} *vs.* -118.4 kJ mol^{-1}) owing to their stronger van der Waals interaction energy (-180.1 kJ mol^{-1} *vs.* -34.6 kJ mol^{-1}), which is mainly attributed to the pi–pi stacking of the aromatic residues with the non-oxidized regions of $C_{20}O_1(OH)_1$ (Fig. 6C). In addition, we noticed that multiple non-polar residues of ghC form favorable hydrophobic interaction with extended non-oxidized regions of $C_{20}O_1(OH)_1$, which is not reflected in the interaction energy. Taken together, ghC module binds to GO with low oxidation degree primarily through pi–pi stacking and hydrophobic interactions.

Conclusions

In this work, the recognition mode of complement protein gC1q with graphene oxide (GO) and self-assembled monolayer (SAM)-coated gold (111) surface and the impacts of surface polarity of these two typical nanomaterials were investigated using molecular dynamics (MD) simulations. The protein gC1q preferentially bind to GO with strong surface polarity ($C_5O_1(OH)_1$) through its ghB module. On the other hand, gC1q tends to bind to GO with weak surface polarity ($C_{20}O_1(OH)_1$) through its ghC module. Similar results are also observed in the adsorption of gC1q on SAM: ghC prefers to bind to nonpolar CH_3-SAM and ghB prefers to bind to charged COO-SAM. The dependence of recognition mode on the surface polarity of GO is mainly attributed to the distinct surface residue composition of ghB and ghC module. There are more charged residues distributed on the surface of ghB module, facilitating formation of hydrogen bonds with GO with higher oxidation degree. By contrast, the surface of ghC module is dominated by non-polar residues, resulting in its tendency to form hydrophobic interactions and pi–pi stacking with GO with large non-oxidized region.

As shown in our work, complement protein gC1q can recognize a variety of foreign intruders with different surface polarities. Moreover, its recognition mode and subsequent immune response can be regulated by surface polarities of intruders. Our results reveal the structural basis of gC1q for the dependence of its recognition mode and the resulting immune response on the surface polarities of nanomaterials (NMs). These findings will be helpful to improve the biocompatibility of NMs by regulating its immune response and provide some theoretical guidance for the application of NMs in the field of biomedicine.

Conflicts of interest

There are no conflicts to declare.

Acknowledgements

The authors gratefully acknowledge Ruhong Zhou, Zonglin Gu, Zhi He, Yichong Lao and Rui Ye for providing comments. This work was supported by National Nature Science Foundation of China (11722434 and 11874319 to J. L., 11675056 and 91730301 to M. Y., 22003057 to X. O.).

References

1 B. Jana, A. Biswas, S. Mohapatra, A. Saha and S. Ghosh, *Chem. Commun.*, 2014, **50**, 11595–11598.
2 T. Bonnard, A. Jayapadman, J. A. Putri, J. Cui, Y. Ju, C. Carmichael, T. A. Angelovich, S. H. Cody, S. French, K. Pascaud, H. A. Pearce, S. Jagdale, F. Caruso and C. E. Hagemeyer, *ACS Nano*, 2018, **12**, 6988–6996.
3 C. Wang, D. Wen and Z. Gu, *Bioconjugate Chem.*, 2018, **29**, 702–708.
4 P. Feng, Y. Chen, L. Zhang, C.-G. Qian, X. Xiao, X. Han and Q.-D. Shen, *ACS Appl. Mater. Interfaces*, 2018, **10**, 4359–4368.
5 A. Y. Mochizuki, I. M. Frost, M. B. Mastrodimos, A. S. Plant, A. C. Wang, T. B. Moore, R. M. Prins, P. S. Weiss and S. J. Jonas, *ACS Chem. Neurosci.*, 2018, **9**, 11–28.
6 R. Chen and J. E. Riviere, *Wiley Interdiscip. Rev. Nanomed.*, 2017, **9**, e1440.

7 K. Pradhan, G. Das, J. Khan, V. Gupta, S. Barman, A. Adak and S. Ghosh, *ACS Chem. Neurosci.*, 2019, **10**, 1535–1543.
8 B. Jana, G. Mondal, A. Biswas, I. Chakraborty, A. Saha, P. Kurkute and S. Ghosh, *Macromol. Biosci.*, 2013, **13**, 1478–1484.
9 M. Xu, J. Zhu, F. Wang, Y. Xiong, Y. Wu, Q. Wang, J. Weng, Z. Zhang, W. Chen and S. Liu, *ACS Nano*, 2016, **10**, 3267–3281.
10 S. F. Kiew, L. V. Kiew, H. B. Lee, T. Imae and L. Y. Chung, *J. Controlled Release*, 2016, **226**, 217–228.
11 J. Chen, X. Shi, L. Ren and Y. Wang, *Carbon*, 2017, **111**, 18–27.
12 X. Jing, H.-Y. Mi, X.-F. Peng and L.-S. Turng, *Carbon*, 2018, **136**, 63–72.
13 C.-M. Tîlmaciu, M. Mathieu, J.-P. Lavigne, K. Toupet, G. Guerrero, A. Ponche, J. Amalric, D. Noël and P. H. Mutin, *Acta Biomater.*, 2015, **15**, 266–277.
14 K. Nomura, S. Mikuni, T. Nakaji-Hirabayashi, M. Gemmei-Ide, H. Kitano, H. Noguchi and K. Uosaki, *Colloids Surf., B*, 2015, **135**, 267–273.
15 S. Klein, M. Kızaloğlu, L. Portilla, H. Park, T. Rejek, J. Hümmer, K. Meyer, R. Hock, L. V. R. Distel, M. Halik and C. Kryschi, *Small*, 2018, **14**, 1704111.
16 M.-A. Shahbazi, M. Hamidi, E. M. Mäkilä, H. Zhang, P. V. Almeida, M. Kaasalainen, J. J. Salonen, J. T. Hirvonen and H. A. Santos, *Biomaterials*, 2013, **34**, 7776–7789.
17 S. Barillet, E. Fattal, S. Mura, N. Tsapis, M. Pallardy, H. Hillaireau and S. Kerdine-Römer, *Nanotoxicology*, 2019, **13**, 606–622.
18 X. Yuan, X. Zhang, L. Sun, Y. Wei and X. Wei, *Part. Fibre Toxicol.*, 2019, **16**, 18.
19 N. B. Alsaleh and J. M. Brown, *Curr. Opin. Toxicol.*, 2018, **10**, 8–14.
20 D. Boraschi, P. Italiani, R. Palomba, P. Decuzzi, A. Duschl, B. Fadeel and S. M. Moghimi, *Semin. Immunol.*, 2017, **34**, 33–51.
21 B. Fadeel, *Front. Immunol.*, 2019, **10**, 133.
22 R. M. Visalakshan, M. N. MacGregor, S. Sasidharan, A. Ghazaryan, A. M. Mierczynska-Vasilev, S. Morsbach, V. Mailänder, K. Landfester, J. D. Hayball and K. Vasilev, *ACS Appl. Mater. Interfaces*, 2019, **11**, 27615–27623.
23 T. Bertok, E. Dosekova, S. Belicky, A. Holazova, L. Lorencova, D. Mislovicova, D. Paprckova, A. Vikartovska, R. Plicka, J. Krejci, M. Ilcikova, P. Kasak and J. Tkac, *Langmuir*, 2016, **32**, 7070–7078.
24 S. A. Sydlik, S. Jhunjhunwala, M. J. Webber, D. G. Anderson and R. Langer, *ACS Nano*, 2015, **9**, 3866–3874.
25 R. Li, L. M. Guiney, C. H. Chang, N. D. Mansukhani, Z. Ji, X. Wang, Y.-P. Liao, W. Jiang, B. Sun, M. C. Hersam, A. E. Nel and T. Xia, *ACS Nano*, 2018, **12**, 1390–1402.
26 Y. Bai, Z. Ming, Y. Cao, S. Feng, H. Yang, L. Chen and S.-T. Yang, *Colloids Surf., B*, 2017, **154**, 96–103.
27 M. Orecchioni, D. Bedognetti, L. Newman, C. Fuoco, F. Spada, W. Hendrickx, F. M. Marincola, F. Sgarrella, A. F. Rodrigues, C. Ménard-Moyon, G. Cesareni, K. Kostarelos, A. Bianco and L. G. Delogu, *Nat. Commun.*, 2017, **8**, 1109.
28 P. C. Henriques, A. T. Pereira, A. L. Pires, A. M. Pereira, F. D. Magalhães and I. C. Gonçalves, *ACS Appl. Mater. Interfaces*, 2020, **12**, 21020–21035.
29 M. V. Carroll and R. B. Sim, *Adv. Drug Deliv. Rev.*, 2011, **63**, 965–975.
30 C. Gaboriaud, P. Frachet, N. M. Thielens and G. J. Arlaud, *Front. Immunol.*, 2012, **2**, 1–8.
31 U. Kishore, R. Ghai, T. J. Greenhough, A. K. Shrive, D. M. Bonifati, M. G. Gadjeva, P. Waters, M. S. Kojouharova, T. Chakraborty and A. Agrawal, *Immunol. Lett.*, 2004, **95**, 113–128.
32 U. Kishore, S. K. Gupta, M. V. Perdikoulis, M. S. Kojouharova, B. C. Urban and K. B. M. Reid, *J. Immunol.*, 2003, **171**, 812–820.
33 A. S. Zlatarova, M. Rouseva, L. T. Roumenina, M. Gadjeva, M. Kolev, I. Dobrev, N. Olova, R. Ghai, J. C. Jensenius, K. B. M. Reid, U. Kishore and M. S. Kojouharova, *Biochemistry*, 2006, **45**, 9979–9988.
34 N. M. Thielens, A. Belime, E. Gravel, S. Ancelet, C. Caneiro, E. Doris and W. L. Ling, *Int. J. Pharm.*, 2018, **536**, 434–439.
35 P. P. Wibroe, S. V. Petersen, N. Bovet, B. W. Laursen and S. M. Moghimi, *Biomaterials*, 2016, **78**, 20–26.
36 Y. Yu, H. Sun, T. Hou, S. Wang and Y. Li, *RSC Adv.*, 2018, **8**, 13997–14008.
37 Y. Xie, W. Gong, J. Jin, Z. Zhao, Z. Li and J. Zhou, *Appl. Surf. Sci.*, 2020, **506**, 144962.
38 S. A. Ragland and A. K. Criss, *PLoS Pathog.*, 2017, **13**, 1–22.
39 M. Saint-Cricq, J. Carrete, C. Gaboriaud, E. Gravel, E. Doris, N. Thielens, N. Mingo and W. L. Ling, *Nano Lett.*, 2017, **17**, 3409–3415.
40 C. Gaboriaud, J. Juanhuix, A. Gruez, M. Lacroix, C. Darnault, D. Pignol, D. Verger, J. C. Fontecilla-Camps and G. J. Arlaud, *J. Biol. Chem.*, 2003, **278**, 46974–46982.
41 Y. Yuan, X. Gao, Y. Wei, X. Wang, J. Wang, Y. Zhang and C. Gao, *Desalination*, 2017, **405**, 29–39.
42 H. Yang, J.-S. Li and X. Zeng, *ACS Appl. Nano Mater.*, 2018, **1**, 2763–2773.
43 P. Sun, Y. Wang, H. Liu, K. Wang, D. Wu, Z. Xu and H. Zhu, *PloS One*, 2014, **9**, e111908.
44 C. Chen, Y.-C. Chen, Y.-T. Hong, T.-W. Lee and J.-F. Huang, *Chem. Eng. J.*, 2018, **352**, 188–197.
45 D. R. Dreyer, S. Park, C. W. Bielawski and R. S. Ruoff, *Chem. Soc. Rev.*, 2010, **39**, 228–240.
46 R. Tian, M. Luo and J. Li, *Phys. Chem. Chem. Phys.*, 2018, **20**, 68–74.
47 J. C. Love, L. A. Estroff, J. K. Kriebel, R. G. Nuzzo and G. M. Whitesides, *Chem. Rev.*, 2005, **105**, 1103–1170.
48 G. A. Kaminski, R. A. Friesner, J. Tirado-Rives and W. L. Jorgensen, *J. Phys. Chem. B*, 2001, **105**, 6474–6487.
49 C.-J. Shih, S. Lin, R. Sharma, M. S. Strano and D. Blankschtein, *Langmuir*, 2012, **28**, 235–241.
50 J. A. L. Willcox and H. J. Kim, *ACS Nano*, 2017, **11**, 2187–2193.
51 W. L. Jorgensen, J. Chandrasekhar, J. D. Madura, R. W. Impey and M. L. Klein, *J. Chem. Phys.*, 1983, **79**, 926–935.
52 M. J. Abraham, T. Murtola, R. Schulz, S. Páll, J. C. Smith, B. Hess and E. Lindahl, *SoftwareX*, 2015, **1–2**, 19–25.

53 G. Bussi, D. Donadio and M. Parrinello, *J. Chem. Phys.*, 2007, **126**, 014101.
54 H. J. C. Berendsen, J. P. M. Postma, W. F. van Gunsteren, A. DiNola and J. R. Haak, *J. Chem. Phys.*, 1984, **81**, 3684–3690.
55 B. Hess, H. Bekker, H. J. C. Berendsen and J. G. E. M. Fraaije, *J. Comput. Chem.*, 1997, **18**, 1463–1472.
56 T. Darden, D. York and L. Pedersen, *J. Chem. Phys.*, 1993, **98**, 10089–10092.
57 W. Humphrey, A. Dalke and K. Schulten, *J. Mol. Graphics*, 1996, **14**, 33–38.
58 R. Kumari, R. Kumar and A. Lynn, *J. Chem. Inf. Model.*, 2014, **54**, 1951–1962.
59 S. Zeng, G. Zhou, J. Guo, F. Zhou and J. Chen, *Sci. Rep.*, 2016, **6**, 24906.